



Long-Term Experience with a 5/15kW-Class Reversible Solid Oxide Cell System

Ro. Peters,^z  M. Frank, W. Tiedemann, I. Hoven, R. Deja, N. Kruse, Q. Fang,  L. Blum, and R. Peters

Forschungszentrum Jülich GmbH, Institute of Energy and Climate Research (IEK-14), 52428 Jülich, Germany

A 5/15 kW-class reversible Solid Oxide Cell (rSOC) system was developed and experimentally investigated at the Forschungszentrum Jülich GmbH. The main component of this system is the well-established Jülich Integrated Module, which consists of four 10-layer SOC sub-stacks with an active cell area per layer of 320 cm². The other necessary system components, such as the evaporator, condenser and blowers are compactly arranged in the vicinity of the Integrated Module. The system's total operation time was more than 9000 h, in detail 2607 h in fuel cells, 6043 h in electrolysis and 448 h in hot standby mode. In fuel cell mode, a power of 5374 W_{DC} at 0.5 A cm⁻² at a fuel utilization of 97.3% was delivered, which resulted in a DC electrical system's efficiency of 62.7% (LHV). Furthermore, in electrolysis mode, a power of -14347 W_{DC} was consumed at 0.89 A cm⁻². At this operating point, the system's DC efficiency reached 70% at a steam utilization of 85%.

© 2021 The Author(s). Published on behalf of The Electrochemical Society by IOP Publishing Limited. This is an open access article distributed under the terms of the Creative Commons Attribution 4.0 License (CC BY, <http://creativecommons.org/licenses/by/4.0/>), which permits unrestricted reuse of the work in any medium, provided the original work is properly cited. [DOI: 10.1149/1945-7111/abcd79]



Manuscript submitted December 4, 2020; revised manuscript received January 12, 2021. Published January 27, 2021.

The fundamental suitability of Solid Oxide Cell (SOC) technology in terms of various electrolysis operating parameters like temperatures, pressures and different gas species has already been shown in several studies.¹⁻⁸

In addition to pure electrolysis operation, reversible Solid Oxide Cell (rSOC) technology has been investigated more intensively in the recent years, because it opens up the possibility of converting and storing regenerative electricity in electrolysis mode as a chemical fuel (for example: hydrogen). And, if necessary, the system can be switched to fuel cell mode to convert the stored chemical energy back into electrical energy as reported, e.g., by Mogensen et al.⁹ Development at the cell and stack levels started in the early 2000 s. For example, Hauch et al.¹⁰ reported on the performance and durability of Solid Oxide Electrolysis Cells (SOECs) and operated cells in both fuel cell and electrolysis modes. In the first 100 h during electrolysis operation, they observed a passivation of the cells, which could be partly regenerated during later fuel cell operation or in long electrolysis operation under constant conditions.

In recent years, work on rSOCs has been significantly intensified. Strohbach et al.¹¹ presented the results of a 20-layer Sunfire stack, where a total of 26 cycles with 12 h of SOFC and SOEC operation were run with an average voltage degradation of 0.06% per cycle. Further stack test results were reported by Tallgren et al.¹² for both operating modes with a 15-layer Elcogen E350 stack with a 121 cm² active electrode area. In electrolysis mode, the stack could be operated at up to -1 A cm⁻² at 675 °C and up to -0.75 A cm⁻² at 650 °C with a steam utilization of up to 80%. Preininger et al.¹³ examined a 10-layer stack with electrolyte-supported cells and open air electrodes with an active cell area of 128 cm² under system-relevant conditions, such as high gas utilization, and operation with hydrogen and carbon containing gases in transient and steady state conditions. In fuel cell mode, a stack efficiency of 68% was achieved and in steam electrolysis mode, a hydrogen production rate of 0.31 h⁻¹ cm⁻² was demonstrated. A comparison of two 10-layer stacks with electrolyte- and fuel electrode-supported cells under steam and CO₂ electrolysis at pressures of up to 8 bar was reported by Riedel et al.¹⁴ It was shown that the ASR of the fuel electrode-supported cell could be significantly reduced by the increase in pressure, while the electrolyte-supported cell showed a minor effect. In addition, it was found that the activation and diffusion resistances

in both stacks were significantly influenced if CO₂ was used for the electrolysis instead of H₂O.

Apart from the investigations at the cell and stack levels, activities relating to the system layout and modeling were also increased. Santhanam et al.^{15,16} showed that, based on a 10-layer stack with an ESC cell in atmospheric operation, a round-trip efficiency of 55% at a reactant utilization of 80% (SOFC) and 88% (SOEC) is possible. When the operating pressure is increased to 30 bar, the round-trip efficiency increases to 60%. This can be further increased if a thermal management system is introduced during endothermic operation. Schauerperl et al.¹⁷ showed that various system layouts react with the fluctuating electricity production from renewable sources. Here, mixtures of hydrogen and methane were examined for the storing and re-powering the electricity. Round-trip efficiencies of about 43% with hydrogen and approximately 32% with methane were also determined.

Furthermore, the first demonstration systems on laboratory and industrial scales were developed. Mougín et al.¹⁸ showed the results of an rSOC system with a 25-layer stack and a 100 cm² active cell area. At an operating temperature of 700 °C and a steam utilization of 78%, a current density of -600 mA cm⁻² was drawn at a cell voltage of 1.3 V, which corresponds to an electrolysis power of about 2 kW. An important outcome of the work was that high steam utilization is the key to high system's efficiency. Later on, Aicart et al.¹⁹ reported that a power of 4.8 kW could be consumed with a 25-layer stack at 800 °C and a steam utilization of 95%. It was also shown that the change between the different operating modes, as well as that between the minimum and maximum power in the same mode could be carried out within 2.5 and 10 min, respectively. Several authors²⁰⁻²³ reported on the recent achievements in system development at Sunfire. To summarize, they showed three realized systems, two of which are rSOCs and one a pressurized electrolysis system. The first ever rSOC system was realized in 2015 by Sunfire together with Boeing. It consumed 80 kW in electrolysis mode and delivered 25 kW in fuel cell mode. A second system consisting of 48 stacks of 30 cells each, arranged in six modules, was developed as part of the GrInHy project. In electrolysis mode, the system consumed a power of 143 kW with an efficiency of 84% based on the lower heating value (LHV) using steam provided by the steel plant. In fuel cell mode, a power of 30 kW at an efficiency of 48% (LHV) was delivered with hydrogen.

The Forschungszentrum Jülich also has a long tradition of developing and operating SOC systems for different areas of application. In the year 2014, the results of a 20 kW SOFC system incorporating four 5 kW stacks, operating with methane and

^zE-mail: ro.peters@fz-juelich.de

reaching a system's efficiency of 41% (LHV), were presented.²⁴ Following this, a thermodynamic analysis of methane-fueled SOFC systems showed that anode off-gas recirculation can increase system's efficiency to more than 61% (LHV).²⁵ Later on, the positive effect of off-gas recirculation could be confirmed during the operation of a 5 kW SOFC subsystem in the laboratory.²⁶ Encouraged by these results, the off-gas recirculation for SOFC operation with pure hydrogen as a fuel was also investigated.²⁷ This study showed that system efficiencies of more than 60% (LHV) can be achieved with this kind of application. In the further course of system development, activities were shifted towards the development of an rSOC system. In this context, a layout of an rSOC system was proposed and investigated in a thermodynamic analysis.²⁸ This system was planned to operate at atmospheric conditions. The produced hydrogen is later compressed to 70 bar and stored in a tank. In fuel cell mode, the efficiency is increased by fuel-side off-gas recirculation with integrated water condensation and reaches 67% (LHV). In electrolysis mode, recirculation is used to increase the hydrogen content at the inlet of the stack to reduce the degradation of the cell. The efficiency in electrolysis mode was optimized by heat recovery and reached 76% (LHV). In this configuration, a round-trip efficiency of 51% can be achieved. Based on this study, an rSOC system (without compressor and storage tank) was designed, built up and tested. While the system was still in operation, a portion of these results were presented at ECS SOFC XVI in Kyoto, Japan.²⁹ In the meantime, the system test was completed and extended and more detailed results are presented in the following sections.

Experimental

To operate the rSOC lab system, a new test environment was built. The housing surrounding this environment is permanently ventilated with an airflow of 11250 slm. This selected air flow guarantees that the entire quantity of hydrogen that the laboratory system can release (regardless of whether it comes from leaks or is generated during electrolysis operation) can be safely discharged without exceeding 50% of the lower explosion limit for hydrogen. In addition, it provides the necessary media, a control system and the corresponding safety equipment to operate the system. A simplified flow diagram of the lab system is shown in Fig. 1.

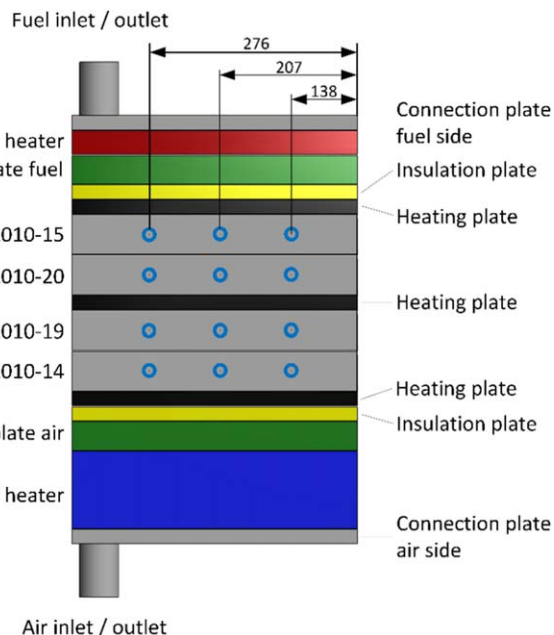


Figure 2. CAD drawing of the Integrated Module. The blue rings mark the positions of the thermocouples in the cell area of the four stacks.

The system components are arranged around the Integrated Module. A recirculation unit is associated with this module, which returns the stack off-gas of the fuel side back to the stack inlet. To overcome the pressure drop of the recirculation loop, a double-headed prototype diaphragm compressor is used. Before the stack off-gas is supplied to the compressor, the steam content is separated from the hydrogen in a plate-type heat exchanger. The resulting heat of condensation is removed via the cooling water. The air side of the system can be supplied with either compressed air from the in-house network or filtered ambient air via a side channel blower. On the fuel side, hydrogen can be supplied by a mass flow controller (MFC) for fuel cell mode as well as steam for electrolysis mode. The demineralized water is fed to an evaporator. Any mixtures of

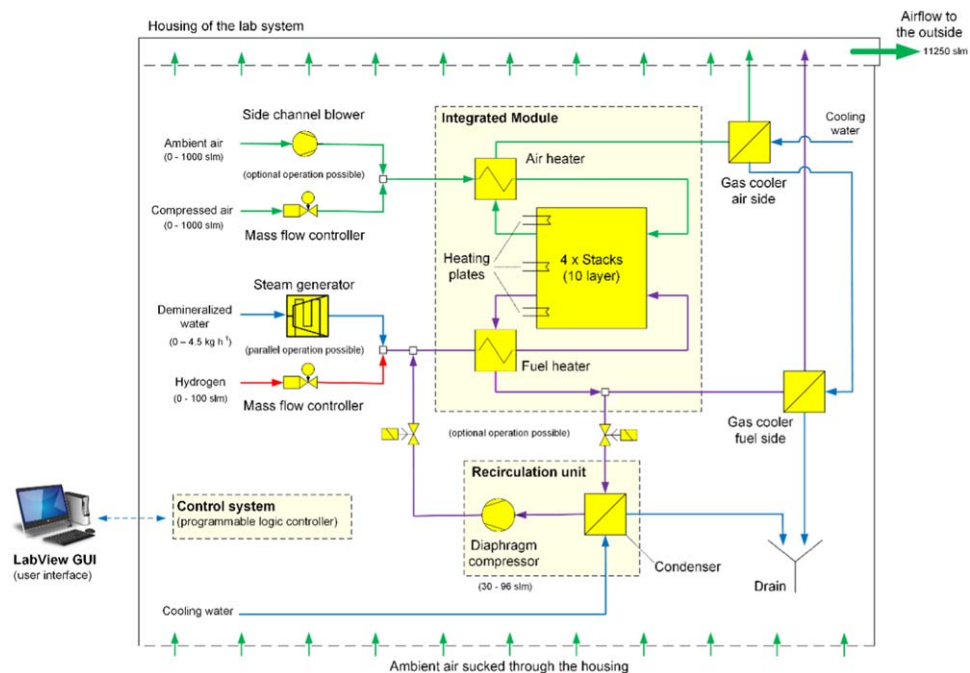


Figure 1. Simplified flow scheme of the laboratory system.

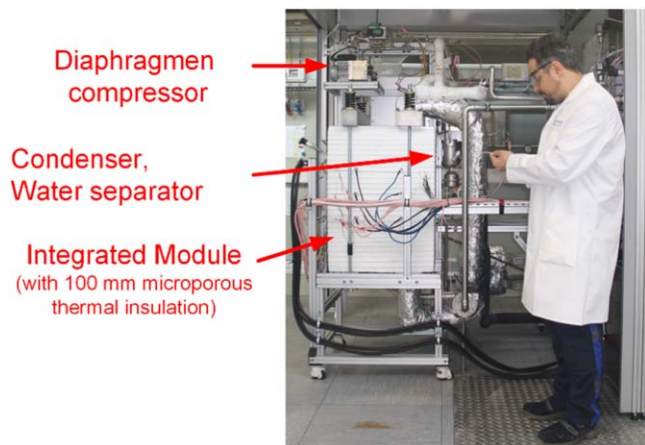


Figure 3. Picture of the main components of the lab system.

hydrogen and steam can be set during operation. After leaving the module, both the air side and the fuel side gas flows are cooled down with heat exchangers and then fed to the ventilation system. All of the necessary control functions are taken over by a programmable logic controller (PLC). A graphical user interface (GUI) programmed in LabView is then used to transfer the desired operating parameters to the PLC and visually depicts the recorded measured values. All supplied media are fed to the lab system at room temperature.

Within the Integrated Module (see Fig. 2) the actual window frame stack design is used. The stack module consists of four sub-stacks with 10 layers each. In each layer, there are four fuel electrode-supported cells based on 8 mol% yttria-stabilized zirconia electrolyte and lanthanum strontium cobalt ferrite (LSCF) air electrode. Each single cell has a size of $10 \times 10 \text{ cm}^2$ and an active electrode area of 80 cm^2 . The metallic components of the stack (e.g. interconnectors, frames, etc.) were made of Crofer22 APU. The air side of the interconnector was coated with a protective coating of manganese cobalt ferrite (MCF) by atmospheric plasma spraying (APS). To improve the contact between cells and interconnectors, a perovskite contact layer was applied on the air side of the cells by screen printing, while Ni mesh was used on the fuel side.

The dimensions of the module are $L \times W \times H$: $22.4 \times 39.9 \times 60 \text{ cm}^3$. The module contains all system components with an operation temperature above $400 \text{ }^\circ\text{C}$.

Two insulating plates are inserted between the heating and baffle plates. These plates are partially filled with a thermal insulation material and are intended to reduce the heat flow between the stacks and the adjacent components. Two connection plates are located on both the top and bottom of the module. These serve as a gas interface between the module and the system.

The module is surrounded on all sides with microporous thermal insulation with a thickness of 10 cm.

In order to provide sufficient force to the mica sealings, the module is loaded with a clamping force of 8000 N applied by conventional coil springs outside of the thermal insulation.

A picture showing the main components of the lab system is presented in Fig. 3. In the foreground, the insulated module and recirculation blower can be seen. The steam generator is mounted on the back side and the condenser including the drain system are on the right side of the module, respectively. The gas supply and control system are located in the surrounding test bench.

Test Results

After the commissioning of the system, a comprehensive test program was commenced on November 12th, 2018. The overall operation time until December 20th, 2019 reached more than 9000 h. An overview of the entire test period is given in Fig. 4.

At the test begin the stationary operating points in the fuel cell and electrolysis mode were examined (up to 2000 h). During this phase, different stationary operating points in fuel cell mode were investigated with and without fuel gas recycling for different fuel utilizations. In electrolysis mode, the current density, temperature and steam utilization were varied, whereby all of these experiments were carried out without recirculation flow (as shown below). This was followed by several days of constant operation in fuel cell mode. After that, the system was cooled down over the turn of the year 2018/2019. Once it was restarted in early 2019, the interaction between the Integrated Module and recirculation loop in fuel cell mode was studied extensively (as shown below). Thereafter, 77 fast switching cycles between fuel cell and electrolysis modes were performed to investigate and optimize the transition procedure (as shown below). Afterwards, the part load behavior of the system for both operating modes was investigated without recirculation flow (as shown below).

As there was no long-term experience with the system in electrolysis mode at Jülich, a long term operation of approximately 4000 h in electrolysis mode followed. This phase was used to determine the degradation behavior of the stack during system operation. Degradation in this phase was determined to be 0.6 mV kh^{-1} and this was in a similar range to the Jülich stack tests during operation in a furnace. After long-term electrolysis operation, the system was switched back to fuel cell mode again. In this phase, increased voltage degradation could be determined. A strongly accelerated voltage drop was observed after roughly 8100 operating hours. At this point, it was decided to switch back to electrolysis mode in order to find out how the system behaved there. A higher voltage degradation was also noticeable in electrolysis mode, but it was significantly lower than in fuel cell operation. The test was stopped after more than 9000 h and the system was cooled down. After the integrated module was dismounted, the stacks were disassembled and examined in a post-mortem analysis. During this examination, various leaks (external and internal), as well as a partial delamination of the air electrode, were observed. The correlation of the respective types of failure to a certain operating point will be the subject of further investigations. The individual operating sections are explained and discussed below.

Stationary results in fuel cell mode.—In the fuel cell mode, the efficiency based on the LHV is determined according to Eq. 1. This efficiency describes the ratio of the generated electrical power of the stack minus the sum of the internal power consumption of the system components, divided by the chemical bonded input power of hydrogen. The efficiency equations were adopted from Frank et al.²⁸ In contrast to the reference, the DC/AC inverter and the power consumption of the supporting control system are not taken into account.

$$\eta_{SOFC, LHV} = \frac{P_{Stack(DC)} - \sum P_{BoP}}{\dot{m}_{H_2, supplied} * LHV_{H_2}} \quad [1]$$

For reasons of comparison with the experimental results, the maximum achievable efficiency in fuel cell mode described by Frank et al.²⁸ is 78.9%. If necessary, the fuel cell efficiency based on the HHV can be determined using Eq. 2.

$$\eta_{SOFC, HHV} = \eta_{SOFC, LHV} * \frac{LHV_{H_2}}{HHV_{H_2}} \quad [2]$$

The system efficiencies achieved during stationary fuel cell operations are shown in Fig. 5. A total of four different operating cases were investigated (two with and two without fuel side recirculation). All of these cases are carried out at a current density of 0.5 A cm^{-2} .

The first operating point (“SOFC 1”) was carried out without recirculation at a stack and system fuel utilization of 70.8%. At this point, a cell voltage of 805 mV and stack power of 5153 W_{DC} was

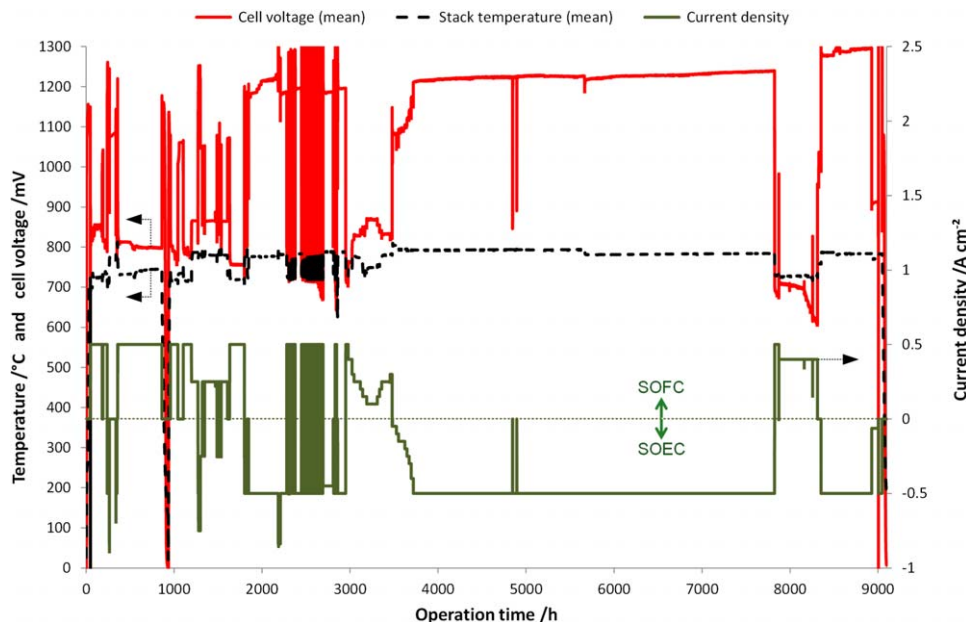


Figure 4. Time plot of the entire test procedure.

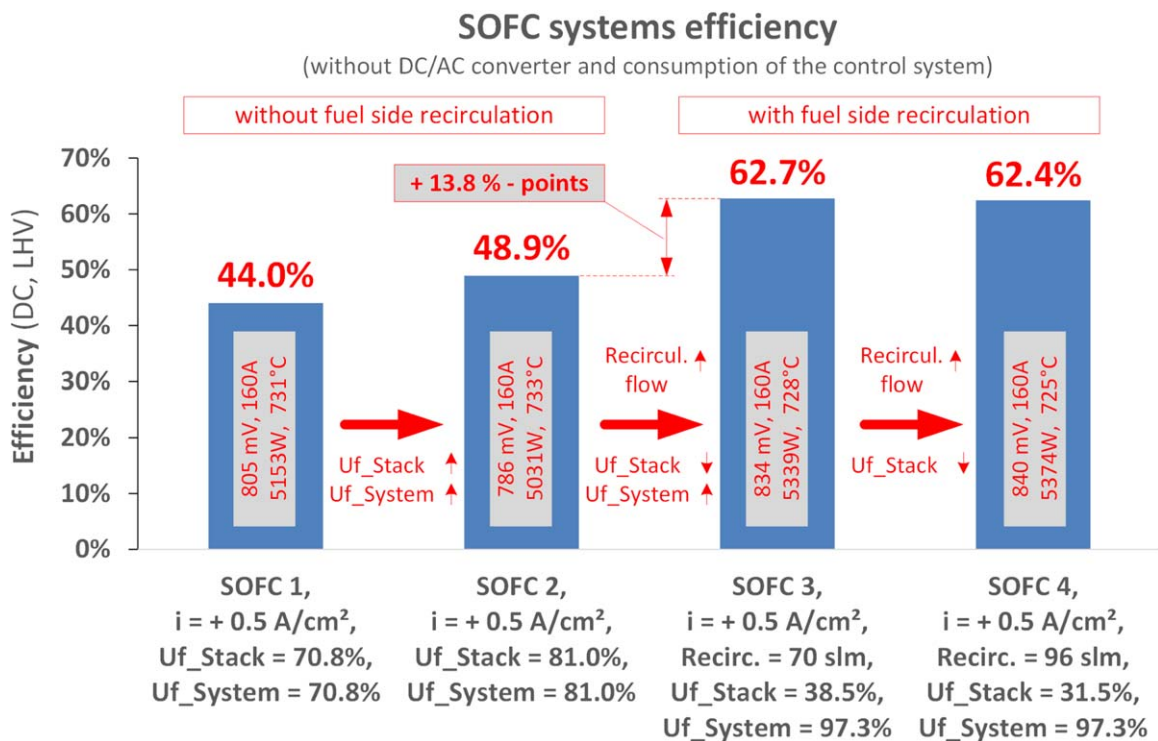


Figure 5. Efficiency in SOFC mode with and without fuel side recirculation.

achieved resulting to an efficiency of 44.0% (LHV). In the next step (“SOFC 2”), the fuel utilization was increased to 81.0%. Although the voltage drops to 786 mV and the stack power to 5031 W_{DC}, the efficiency increases to 48.9% (LHV), because less hydrogen had to be supplied to the system. Subsequently, the system efficiencies including recirculation were determined. At the operating point “SOFC 3” a system fuel utilization of 97.3% was realized at a recirculation quantity of 70 slm. Due to recirculation, the stack fuel utilization was reduced to 38.5% in a single pass. Compared to the operating points without recirculation, the cell voltage rises to 834 mV, and therefore the stack power increases to 5339 W_{DC}. This increase is caused by the increased Nernst voltage due to the

higher average hydrogen concentration in the stack. At this operating point, an efficiency of 62.7% (LHV) was reached. In the last step (“SOFC 4”), the volume flow on the recirculation loop is increased from 70 to 96.2 slm, while maintaining the same system fuel utilization. At the same time, the cell voltage (840 mV) and stack power (5374 W_{DC}) increase slightly, again due to a rising Nernst voltage, but the efficiency drops from 62.7% to 62.4% (LHV). Due to the higher recirculation flow and the resulting increased pressure loss on the recirculation loop, the power consumption of the diaphragm compressor simultaneously increases. The negative effect of the compressor power consumption overcompensates the positive effect of the cell voltage increase. If one compares the highest values

without recycling (“SOFC 2”) and with recycling (“SOFC 3”), it becomes obvious that the recirculation increases the efficiency by a total of 13.8 percentage points.

In Fig. 6, the temperature distribution in the four stacks is shown by way of example for case “SOFC 3” with a recirculation flow of 70 slm. The mean temperature of the stacks was 728 °C. As the stack is operated in co-flow, the lowest temperatures are found on the gas inlet side. The temperature difference between the inlet and outlet of the cell area was about 150 °C. It can also be seen that the temperatures of the top stack (F^{Y8}2010–15) and the bottom stack (F^{Y8}2010–14) are about 25 °C lower than the two middle ones. A part of the heat produced by the two outer stacks is given by radiation to the adjacent module components, and therefore they have lower temperatures, although the amount of air is the same for all stacks.

Stationary results in electrolysis mode.—In electrolysis mode, the efficiency based on the LHV is determined according to Eq. 3. This efficiency describes the ratio of the chemical bonded power of the produced hydrogen, divided by the consumed electrical power of the stack plus the sum of the internal power consumption of the system components. In contrast to the reference, the AC/DC inverter and the power consumption of the supporting control system are not taken into account.

$$\eta_{SOEC, LHV} = \frac{\dot{m}_{H_2, produced} * LHV_{H_2}}{P_{Stack (DC)} + \sum P_{BoP}} \quad [3]$$

The maximum achievable efficiency in electrolysis mode mentioned by Frank et al.²⁸ is 84.6%

In addition, the electrolysis efficiency based on the HHV can be determined using Eq. 4.

$$\eta_{SOEC, HHV} = \eta_{SOEC, LHV} * \frac{HHV_{H_2}}{LHV_{H_2}} \quad [4]$$

Three different operating points were taken into account when determining the efficiency (see Fig. 7). All of these were run without a recirculation flow, because in the present configuration (recirculation including steam condensation) will not increase the system’s efficiency in the electrolysis mode. The operating points differ in steam utilization, stack current and heating plate temperature. At operating point “SOEC 1,” a current density of -0.5 A cm^{-2} was run at 70% steam utilization and a heating plate set point temperature of 730 °C. For “SOEC 2,” the current density was increased to -0.84 A cm^{-2} and the steam utilization to 80%. At the

same time, the set point of the heating plate was increased to 830 °C. At the operating point “SOEC 3,” the maximum amount of steam available in the test bench is supplied to the stack. By that, the current density was increased slightly to -0.89 A cm^{-2} and the steam utilization to 85%.

In operating point “SOEC 1,” a stack power of -8133 W_{DC} was consumed at a system’s efficiency of 67.5% (LHV). In the case of “SOEC 2,” a stack power of -13303 W_{DC} resulted with an efficiency of 69.3% (LHV). With “SOEC 3” a power of -14347 W_{DC} with an efficiency of 70% (LHV) was drawn. The cell voltage remains approximately constant in all three operating points, although the current is significantly increased. This can be explained by reference to the stack temperature, because operating point “SOEC 1” was performed at a 730 °C set point temperature of the heating plates, whereas points “SOEC 2” and “SOEC 3” had a set point of 830 °C. The results indicate that the system’s efficiency increases with higher steam utilization and higher stack power.

The temperature distribution of the stack for operating point “SOEC 3” is shown in Fig. 8. The mean temperature of the stacks was 761 °C. The Temperature difference between the inlet and outlet of the cell area was about 55 °C and was thus only about a third as high as during fuel cell operation. Moreover, the temperature distribution in the four stacks lies much closer together, because the heat transfer to the neighboring components was compensated for by the heating plates.

In electrolysis mode, the stacks operate below the thermo-neutral voltage, which means, that heat must be supplied continuously via the heating plates. In this case, the heating plates shield the heat transfer between the stacks and other module components. The lower temperature gradient between the inlet and outlet of the cell area can be explained by the fact that the amount of air flow through the stack is significantly reduced compared to fuel cell operation.

Influence of fuel side recirculation in fuel cell mode.—In this chapter, the influence of fuel side recirculation on the system’s efficiency and fuel utilization in fuel cell mode is examined. In a first step, the system fuel utilization was gradually increased by reducing the hydrogen supply for a constant recirculation flow rate of 50 slm. During this test series, the gas composition of the recirculation flow was measured with a gas chromatograph.

Because of the low steam condensation temperature in the condenser, it would be expected that almost only hydrogen was measured. However, the actual measurement results showed large amounts of nitrogen at high system fuel utilization. Figure 9a shows

SOFC stack temperatures for case SOFC 3

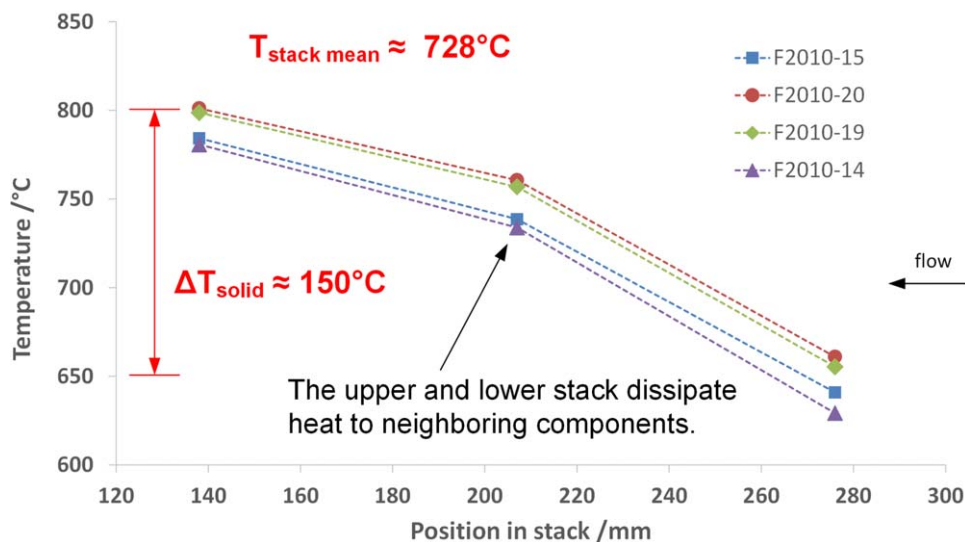


Figure 6. Temperature distribution in the cell area of the stacks for the case of “SOFC 3.” The blue rings in Fig. 2 indicate the positions of the thermocouples in the stacks.

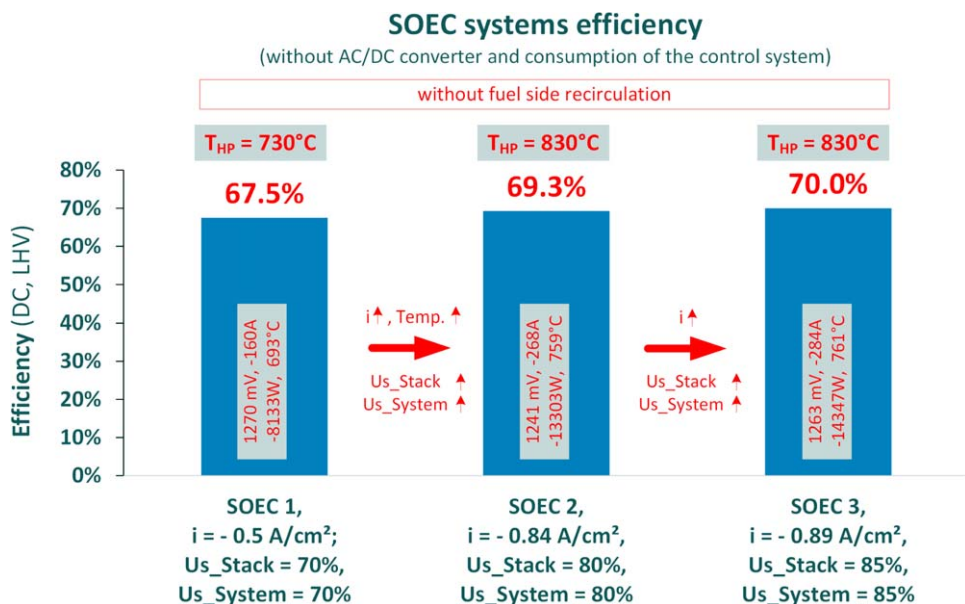


Figure 7. Efficiency in SOEC mode without recirculation.

SOFC stack temperatures for case SOEC 3

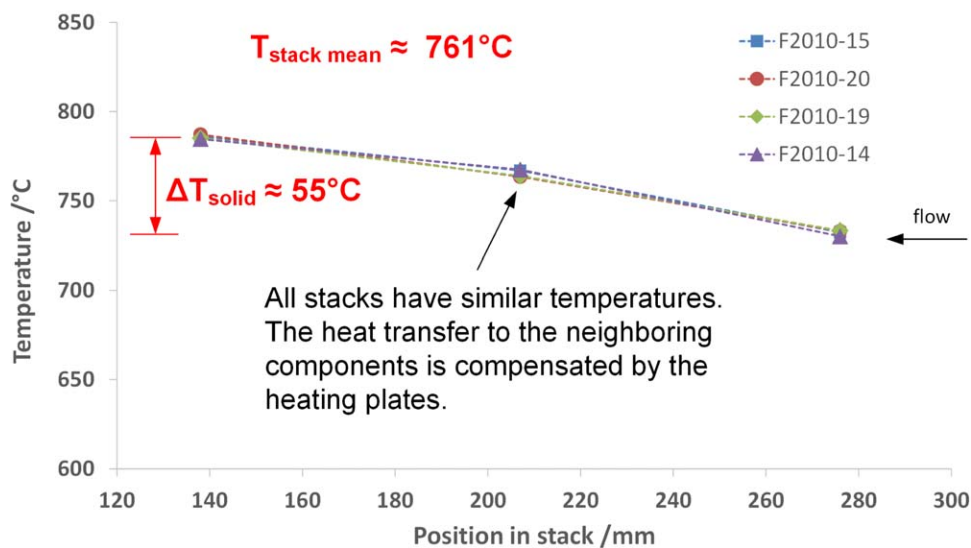


Figure 8. Temperature distribution of the stack for operation point “SOEC 3.” The blue rings in Fig. 2 indicate the positions of the thermocouples in the stacks.

the measured nitrogen concentration and pressure drop on the recycle loop.

In addition, due to the steadily decreasing hydrogen concentration, the Nernst voltage and so the cell voltage decreased with the increasing system fuel utilization (see Fig. 9b).

The influence on the system’s efficiency is shown in Fig. 9c. It can be seen that the system’s efficiency increases with increasing fuel utilization. If the fuel utilization is greater than 95%, the efficiency increases much more slowly, and even drops again later. This effect can be explained by the drop in cell voltage and the simultaneous increase in blower power.

As the blower power has an influence on the system’s efficiency, in a second step, the recirculation flow rate was sought, which enables the highest possible system’s efficiency to be achieved. From the previous experiment, it was already shown that the nitrogen concentration in the fuel gas rises sharply with very high fuel gas utilization. Therefore, in this test series, the recirculation flow was varied at a constant system fuel utilization of 95% (see Fig. 9d). As the recirculation flow increases, the system’s efficiency

initially also does. It was observed that the performance of the recirculation blower also continuously increased, as a higher flow rate had to be conveyed with a higher compression pressure. In contrast, the power consumption of the air blower continuously dropped. Here, the amount of air fed into the system was continuously reduced, as an increasing proportion of the stack cooling was taken over by the recirculation flow. The efficiency continuously increased up to a recycling flow of 80 slm. It then dropped again because the positive effect of the Nernst voltage increase was overcompensated for by the power consumption of the blowers.

Part load operation in fuel cell and electrolysis modes.—The part load behavior in fuel cell and electrolysis mode was also examined in detail. This test series in fuel cell mode was carried out without recirculation flow and at a constant fuel utilization of 70% at a time when the stacks had already suffered partial degradation. For this reason, the efficiencies achieved in fuel cell operation were lower than described in Fig. 5. In electrolysis mode, a recycling rate

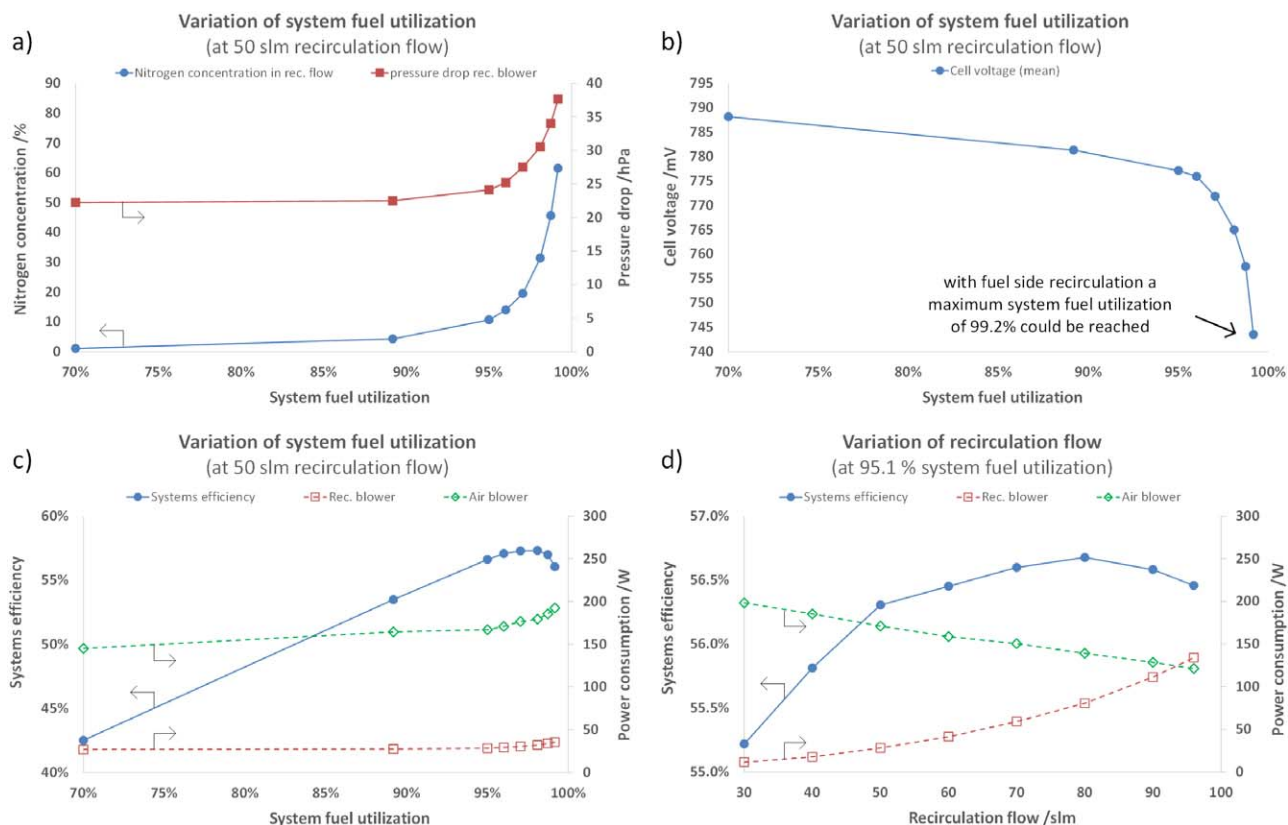


Figure 9. Variation of system fuel utilization and recirculation flow. (a) gas concentration and pressure drop over system fuel utilization; (b) cell voltage over system fuel utilization; (c) system’s efficiency and power consumption of the blowers over the system’s fuel utilization; (d) system’s efficiency over the recirculation flow.

of 30 slm and steam utilization of 70% were set. Because of operation below the thermo-neutral voltage, the heating plates were always run with a set-point temperature of 820 °C. The current densities were varied from +0.1 to +0.5 A cm⁻² in fuel cell operation and from -0.05 A cm² to -0.5 A cm² in electrolysis mode. The results are shown in Fig. 10.

In fuel cell operation without heating plate support, the efficiency continuously increased up to a partial load of 20%. When the load was reduced, the cell voltage continuously increased and so the electrochemical heat production fell at the same time. This means that less air had to be supplied to cool the stack, which resulted in less power consumption by the air blower. These two positive effects led to an increase in the system’s efficiency. As the temperature of the stack remained relatively constant, even under partial load, the

heat losses of the integrated module also remained constant. At 30% partial load, the heat production in the stack became so low that, in combination with the superimposed heat losses, the minimum air excess ratio of two was achieved. For this reason, the load could not be reduced any further.

The electrolysis test series was always operated with the heating plates switched on (set point: 820 °C) due to the operation below the thermo-neutral voltage at a constant steam utilization of 70%. In contrast to the fuel cell operation, 30 slm (minimum flow rate of the recirculation blower) of hydrogen was always recycled here to ensure a sufficient hydrogen concentration at the entry of the cell. The amount of air was also kept constant at 50 slm so that the oxygen concentration at the stack outlet did not rise too high. The total power consumption of the two blowers varied between

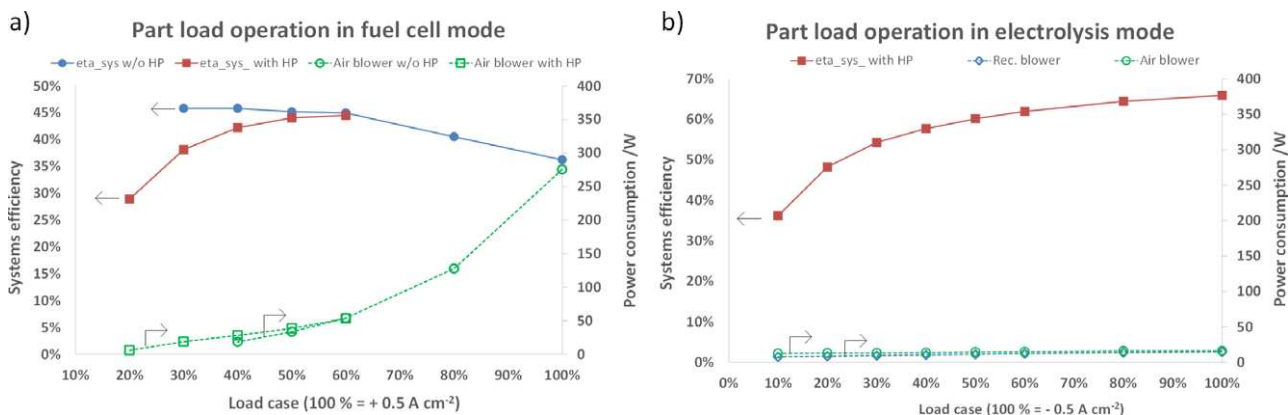


Figure 10. Partial load behavior in: (a) fuel cell mode with and without the support of the heating plates; and (b) electrolysis mode with the support of the heating plates.

20–30 W and was therefore mostly significantly lower than in fuel cell operation. Nevertheless, the efficiency dropped as the load decreased. This can be explained by the permanent heat losses. These heat losses also remained almost constant because of the constant stack temperature and must be compensated by the heating plates. According to Eq. 3, the efficiency must then decrease, as at partial load $\sum P_{BoP}$ increases, with the ratio $\dot{m}_{H_2, produced}$ to $P_{Stack(DC)}$ remaining almost the same. In fact, the cell voltage dropped slightly towards the partial load, but this was compensated by the increasing heating power in a neutral manner. In this series of measurements, 10% represents the minimum partial load, because below this power level no stable steam generation could be guaranteed.

Switching between fuel cell und electrolysis modes.—In addition to the investigation of the stationary operating points, the transient operation while switching from fuel cell to electrolysis mode was analyzed. For this purpose, a corresponding switching procedure was developed and tested. The individual steps are described below and illustrated in Fig. 11.

The switching procedure began when the system was run in fuel cell mode. At minute 15 (point 1 in Fig. 11), the procedure was initiated. The required amount of demineralized water was added (upper diagram, red line) to the steam generator and the heating plates are turned on with a set point temperature of 830 °C. Immediately after the set point change, the power consumption of the heating plates increases drastically (lower diagram, blue line). From this point on, a waiting period of 10 min was required to achieve stable and reliable steam production. During this waiting time, the steam content on the fuel side increased, which was why the mean cell voltage and, in consequence, the stack power decreased slightly at the same current density (lower diagram, red dashed lines). From minute 24 on, in fuel cell operation, the load was reduced towards zero. In minute 25 (point 2), the fuel cell operation was finished and electrolysis operation begins. At the same time, the hydrogen (upper diagram, blue line), air (upper diagram, purple-dashed line) and recirculation flow (upper diagram, black-dotted

line) are reduced or switched off and the current is increased stepwise to the full electrolysis operation of -160 A. At minute 26.5, the full electrolysis current was reached, and this operating point is maintained until minute 86. In minute 40, the heating plate power has stabilized at a constant level. This means that it took roughly 25 min to almost convert the temperature distribution of the fuel cell operation (Fig. 6) into the temperature profile of the electrolysis operation (Fig. 8). However, due to the thermal mass of the stack, the average stack temperature increases by further 23 °C and the mean cell voltage drops by about 55 mV until minute 86 was reached.

Subsequently, the electrolysis power and the amount of water are gradually reduced, while the hydrogen, air and recirculation flow are increased. The heating plates are switched off at this point, by entering a low set point temperature. At minute 87.5 (point 3), the electrolysis mode changes to fuel cell mode again. Subsequently, the air volume flow had to be adjusted several times to control the stack temperature. The actual change from full electrolysis to full fuel cell operation can be done in less than three minutes. The reverse step took 13 min, because of the 10 min waiting period for stable steam production before electrolysis mode operation could be commenced.

Conclusions

A highly efficient rSOC system was built and experientially investigated. An overall system operation time of more than 9000 h was achieved under varying conditions.

The maximum delivered power in fuel cell mode was 5374 W_{DC}. The maximum achieved electrical DC efficiency in fuel cell mode at nominal load was 62.7% (LHV). This high value is achieved by integrating a fuel side recirculation loop, including steam condensation. The highest system fuel utilization measured during the experiment was 99.2%. The maximum system's efficiency was achieved with a system fuel utilization of 97.3%. In the electrolysis mode, a maximum power of -14347 W_{DC} at a steam utilization of

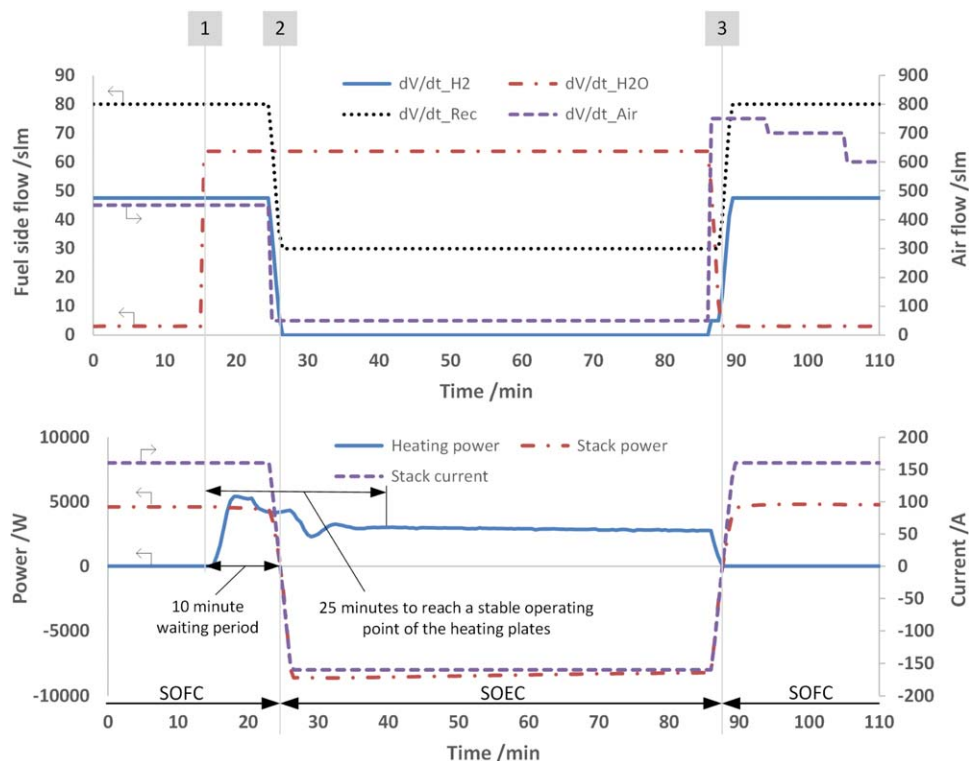


Figure 11. Switching procedure between fuel cell and electrolysis mode. From full fuel cell operation with a stack current of 160 A, the system is switched to electrolysis operation with -160 A. After 60 min under these operating conditions, it has been switched back to the fuel cell operation with 160 A. The upper part of the diagram shows the gas flows and the lower part the stack current, the power of the stacks and the heating plates.

85% was consumed. Thereby, the maximum electrical DC efficiency was 70% (LHV).

An examination of the part-load behavior showed that in fuel cell mode, a minimum part-load current density of 20% (based on 0.5 A cm^{-2}), and in electrolysis mode 10%, could be achieved. It was shown that switching between the two operating modes could generally be realized in less than three minutes. However, when switching from fuel cell to electrolysis mode, a period of 10 min must transpire in order to achieve stable evaporation in the steam generator. This indicates that the steam generator must be improved in terms of its dynamic behavior if shorter switching times are required. During 4000 h of steady state electrolysis operation a voltage degradation of $0.6\% \text{ kh}^{-1}$ was observed.

The system test demonstrated the feasibility of a highly efficient and dynamic reversible SOC system. However, the long-term stability, especially in fuel cell mode, requires further investigation.

In the next step, it is planned to build and operate a 10/40 kW rSOC system in early 2021.

Acknowledgments

The authors would like to thank their colleagues at the Forschungszentrum Jülich GmbH, who helped to realize the system and to the Helmholtz Society for financing these activities. Special thanks go to Rabah Lekehal and Stefan Küpper for their support in the construction of the lab system.

ORCID

Ro. Peters  <https://orcid.org/0000-0002-7587-1762>

Q. Fang  <https://orcid.org/0000-0002-2812-6866>

References

1. R. Küngas, *J. Electrochem. Soc.*, **167**, 044508 (2020).
2. M. Riedel, M. P. Heddrich, and K. A. Friedrich, *J. Electrochem. Soc.*, **167**, 024504 (2020).
3. A. Hauch, R. Küngas, P. Blennow, A. B. Hansen, J. B. Hansen, B. V. Mathiesen, and M. B. Mogensen, *Science*, **370**, eaba6118 (2020).
4. S. Megel et al., *ECS Trans.*, **78**, 3089 (2017).
5. A. Hagen and H. L. Frandsen, *ECS Trans.*, **91**, 235 (2019).
6. A. Hagen and P. V. Hendriksen, *ECS Trans.*, **78**, 145 (2017).
7. H. Uchida, H. Nishino, P. Puengjinda, and K. Kakinuma, *J. Electrochem. Soc.*, **167**, 134516 (2020).
8. P. Kazempoor, C. Wendel, and R. J. Braun, *ECS Trans.*, **58**, 45 (2014).
9. M. B. Mogensen et al., *Clean Energy*, **3**, 175 (2019).
10. A. Hauch, S. H. Jensen, S. Ramousse, and M. Mogensen, *J. Electrochem. Soc.*, **153**, A1741 (2006).
11. T. Strohbach, F. Mittmann, C. Walter, D. Schimanke, and C. Geipel, *ECS Transactions*, **68**, 125 (2015).
12. J. Tallgren, O. Himanen, and M. Noponen, *ECS Trans.*, **78**, 3103 (2017).
13. M. Preininger, B. Stoeckl, V. Subotić, F. Mittmann, and C. Hochenauer, *Appl. Energy*, **254**, 113695 (2019).
14. M. Riedel, M. P. Heddrich, A. Ansar, Q. Fang, L. Blum, and K. A. Friedrich, *J. Power Sources*, **475**, 228682 (2020).
15. S. Santhanam, M. P. Heddrich, M. Riedel, and K. A. Friedrich, *Energy*, **141**, 202 (2017).
16. S. Santhanam, M. Heddrich, M. Riedel, and K. A. Friedrich, *ECS Trans.*, **78**, 2925 (2017).
17. R. Schauerperl, B. Defner, J. Rechberger, and N. Soukup, *ECS Trans.*, **78**, 2933 (2017).
18. J. Mougín, S. Di Iorio, A. Chatroux, T. Donnier-Marechal, G. Palcoux, M. Petitjean, and G. Roux, *ECS Trans.*, **78**, 3065 (2017).
19. J. Aicart, S. Di Iorio, M. Petitjean, P. Giroud, G. Palcoux, and J. Mougín, *Fuel Cells*, **19**, 381 (2019).
20. K. Schwarze, O. Posdziech, S. Kroop, N. Lapeña-Rey, and J. Mermelstein, *ECS Trans.*, **78**, 2943 (2017).
21. J. Mermelstein and O. Posdziech, *Fuel Cells*, **17**, 562 (2017).
22. O. Posdziech, K. Schwarze, and J. Brabandt, *Int. J. Hydrogen Energy*, **44**, 19089 (2018).
23. O. Posdziech, T. Geißler, K. Schwarze, and R. Blumentritt, *ECS Trans.*, **91**, 2537 (2019).
24. R. Peters, L. Blum, R. Deja, I. Hoven, W. Tiedemann, S. Küpper, and D. Stolten, *Fuel Cells*, **14**, 489 (2014).
25. M. Engelbracht, R. Peters, L. Blum, and D. Stolten, *J. Electrochem. Soc.*, **162**, F982 (2015).
26. R. Peters, M. Engelbracht, W. Tiedemann, I. Hoven, R. Deja, V. N. Nguyen, L. Blum, and D. Stolten, *ECS Trans.*, **78**, 2489 (2017).
27. R. Peters, R. Deja, M. Engelbracht, M. Frank, V. N. Nguyen, L. Blum, and D. Stolten, *J. Power Sources*, **328**, 105 (2016).
28. M. Frank, R. Deja, R. Peters, L. Blum, and D. Stolten, *Appl. Energy*, **217**, 101 (2018).
29. R. Peters, M. Frank, W. Tiedemann, I. Hoven, R. Deja, V. N. Nguyen, L. Blum, and D. Stolten, *ECS Trans.*, **91**, 2495 (2019).